

A genetic interaction map of cell cycle regulators

Maximilian Billmann^{1,4}, Thomas Horn^{1,4}, Bernd Fischer^{2,3}, Thomas Sandmann¹,
Wolfgang Huber² and Michael Boutros^{1,*}

¹German Cancer Research Center (DKFZ), Division Signaling and Functional Genomics and
Heidelberg University, Department of Cell and Molecular Biology,
Im Neuenheimer Feld 580, 69120 Heidelberg, Germany

²EMBL, Genome Biology Unit, Meyerhofstr. 1, 69118 Heidelberg, Germany

³German Cancer Research Center (DKFZ), Computational Genome Biology

⁴These authors contributed equally

*Address for correspondence

Phone: +49 6221 421951

Fax: +49 6221 421959

Email: m.boutros@dkfz.de

ABSTRACT

Cell based RNAi is a powerful approach to screen for modulators of many cellular processes. However, resulting candidate gene lists from cell-based assays comprise diverse effectors, both direct and indirect, and further dissecting their functions can be challenging. Here, we screened a genome-wide RNAi library for modulators of mitosis and cytokinesis in *Drosophila* S2 cells. The screen identified many previously known genes as well as modulators that have previously not been connected to cell cycle control. We then characterized ~300 candidate modifiers further by genetic interaction analysis using double RNAi and a multiparametric, imaging-based assay. We found that analyzing cell-cycle relevant phenotypes increased the sensitivity for associating novel gene function. Genetic interaction maps based on mitotic index and nuclear size grouped candidates into known regulatory complexes of mitosis or cytokinesis, respectively, and predicted previously uncharacterized components of known processes. For example, we confirmed a role for the *Drosophila* CCR4 mRNA processing complex component *l(2)NC136* during the mitotic exit. Our results show that the combination of genome-scale RNAi screening and genetic interaction analysis using process-directed phenotypes provides a powerful two-step approach to assign components to specific pathways and complexes.

Keywords: Synthetic genetic interactions, RNAi, multiparametric analysis, automated imaging, cell cycle regulation

BACKGROUND

Large-scale genetic screens have identified components of many biological processes in a broad spectrum of organisms (Patton and Zon, 2001; Jorgensen and Mango, 2002; St Johnston, 2002; Boutros and Ahringer, 2008). Such experiments have considerably expanded our knowledge of regulatory complexes and pathways. In recent years, classical genetic screens have been complemented by cell-based, loss-of-function experiments using RNAi (Kiger *et al.*, 2003; Boutros *et al.*, 2004; Carpenter and Sabatini, 2004; Kittler *et al.*, 2004; DasGupta *et al.*, 2005). While screening technologies have made significant advances, moving from candidate ‘hit’ lists to precise delineation of functional relationships has remained challenging. Prioritization of candidates for follow-up experimentation often relies on prior knowledge, leaving uncharacterized genes untouched. Therefore, systematic and scalable secondary lines of screens are necessary to group candidates into functional categories, pathways or complexes.

In yeast, systematic double-perturbation experiments, termed SGA (synthetic genetic arrays), dSLAM or E-MAPs (Pan *et al.*, 2004; Tong *et al.*, 2004; Schuldiner *et al.*, 2005), have been employed to explore diverse biological processes and have successfully identified previously undiscovered functional relationships (Tong *et al.*, 2004; Schuldiner *et al.*, 2005; Collins *et al.*, 2007). Both in *S. cerevisiae* and in *S. pombe*, large collections of mutant alleles are available to generate maps of biological processes and compare their phylogenetic relationships (Dixon *et al.*, 2008; Roguev *et al.*, 2008; Jonikas *et al.*, 2009). The largest scale synthetic genetic interaction study to date has generated genetic interaction profiles for about 75% of the yeast genome (Costanzo *et al.*, 2010). While full genome genetic interaction analysis has not yet been approached in metazoan cells, the concept of systematic co-depletion and quantitative analysis has been applied in *C. elegans* (Lehner *et al.*, 2006; Tischler *et al.*, 2008), *Drosophila* cells (Bakal *et al.*, 2008; Horn *et al.*, 2011; Fischer *et al.*, 2015) as well as mouse (Roguev *et al.*, 2013) and human cell lines (Laufer *et al.*, 2013; Wang *et al.*, 2014).

Here, we describe a two-stage approach that first prioritizes genes by genome-wide screening for subsequent medium-scale, imaging-based synthetic genetic interaction (SGI) analysis. We screened for modulators of cell cycle regulation by genome-wide RNAi and high-throughput imaging of *Drosophila* cells. Then, we used double RNAi to systematically map the functional relationships between these genes. This analysis grouped genes into functional modules, and generated hypotheses for the function of genes not previously implicated in cell cycle regulation, including *CG11753* (*Drosophila* *SYS1*) and *l(2)NC136* (*Drosophila* *CNOT3*). Taken together, this study demonstrates the use of synthetic genetic interaction experiments in metazoan cells to refine functional predictions from large-scale perturbation experiments.

RESULTS AND DISCUSSION

A two-step RNAi screening approach for regulators of the cell cycle

To identify and map potentially novel regulators of the cell cycle we used high-throughput imaging to measure the effects of single and double perturbations on cell-cycle relevant phenotypes in *Drosophila* S2 cells (Figure 1A, Material and Methods). First, using a genome-wide RNAi library targeting ~98% of the protein coding transcripts (Horn *et al.*, 2010; Horn and Boutros, 2013) we systematically interrogated the *Drosophila* genome for effects of single gene knock downs on the cell cycle. Fluorescence microscopy images of nuclei (DNA) and phospho-Histone H3-positive (pH3, phosphorylated from mitotic prophase to anaphase) cells were captured for each condition after five days knock down. We focused our analysis on three phenotypes extracted from the images: number of nuclei ('cell number') as a measure of cell viability, and average nuclear area as well as the mitotic index (proportion of pH3-positive cells) as measurements directly related to cell cycle relevant processes (Materials and Methods). After selecting a set of ~300 putative novel cell cycle regulators from the genome-wide dataset, in a second experiment we tested double knockdowns of the candidates with 14 well-characterized cell cycle regulators using the same microscopic readouts and assessed genetic interactions. That way we aimed at mapping the putative novel regulators to known cell cycle processes.

Results of the genome-wide screen

To identify RNAi reagents that had effects on the cells in the genome-wide screen z-scores were computed for each of the three phenotypes. For nuclear area and mitotic index phenotypes we adjusted for cell count effects using regression analysis (Materials and Methods). The z-scores of two replicates showed strong positive correlations for all three phenotypes (Supplemental Figure 1A). By comparing z-scores between the three phenotypes across the entire screen we found that they provided complementary information about the effects of gene knockdowns as indicated by their low Pearson correlation (Supplemental Figure 1B). Figure 1B highlights the information gain by assessing nuclear area and mitotic index in addition to cell count: while genes implicated in different biological processes affected cell counts similarly (or had no effect at all), they showed differential effects in the other phenotypes. For example, knocking down genes encoding sperm-specific dynein intermediate chains (*Sdic1*, *Sdic2*, *Sdic3*, *Sdic4*) or genes involved in mRNA cleavage and polyadenylation (*Cpsf100*, *Cpsf160*, and *Cpsf73*) showed mild to no effects on cell counts, but the mitotic index was increased after perturbation of the dynein intermediate chains and decreased after perturbation of the mRNA processing factors (Figure 1C). This was also in agreement with their known implications in the cell cycle where dyneins are required for mitotic progression, and mRNA processing factors are important during interphase (Manley, 1995; Nurminsky *et al.*, 1998). In another example we found that genes with a role in cytokinesis could have diverging effects on the mitotic index (increased for *tum*, *pbl*, *zip*, and *scra*; decreased for *Incep*, *borr*, *Det*, and *ial*), while invariably decreasing cell counts and increasing nuclear area (Figure 1C). This confirmed the requirement of the components of the chromosomal passenger complex Incep (inner centromere protein), Borr (borealin, *Drosophila*

CDCA8), and Det (deterin, *Drosophila* survivin) for Histone H3 phosphorylation by ial (aurB, aurora B kinase) (Carmena *et al.*, 2012), in contrast to the proteins tum (tumbleweed, *Drosophila* RACGAP1) and pbl (pebble, *Drosophila* ARHGEF5) that are essential for cytokinesis but do not alter phospho-Histone H3 phosphorylation (Zavortink *et al.*, 2005). Overall, assessing the three complementary phenotypes provided a more detailed view on gene functions and highlighted genes with potential roles in cell cycle.

To get a more comprehensive picture of factors affecting nuclear area and mitotic index as markers of cell cycle progression we filtered the results of the genome-wide screen for all treatments with an absolute z-score ≥ 3 for either of the phenotypes. Of $\sim 15,000$ genes assessed by RNAi (Supplemental Table S1), knockdowns of $\sim 1,000$ (6.7%) resulted in such a phenotype (Supplemental Table S2). About 17% of them were specific to nuclear area, 75% to mitotic index, and 8% scored in both phenotypes. We grouped the phenotypic profiles of the 1,000 genes by hierarchical clustering of their z-scores (Figure 2A). This identified several clusters that were enriched for known cell cycle regulators (Figure 2B-E). For example cluster I (Figure 2B) grouped proteins required for formation of the mitotic spindle (Teixido-Travesa *et al.*, 2012) including tubulins as well as components of the augmin and CCT chaperonin complexes (Supplemental Table S3). Loss of function of these proteins commonly increased the mitotic index indicating a mitotic arrest. In contrast cluster IV (Figure 2E) grouped components of the COP9 signalosome (CSN) (Supplemental Table S3) complex, which is required during the G1/S transition of the cell cycle (Doronkin *et al.*, 2003). Knocking down CSN members commonly decreased the mitotic index, indicating a cell cycle arrest before mitosis. To address more systematically the question which processes could be detected by our assay we manually annotated a high-confidence list of 131 proteins with well-characterized roles during G1/S transition, the G2/M checkpoint, the mitotic spindle, as well as regulators of mitotic progression and cytokinesis (Supplemental Table S3). We found that 96 of the known factors (73%), covering all manually annotated cell cycle processes, had an absolute z-score ≥ 3 in nuclear area and/or mitotic index (Supplemental Figure 2A), which validated our screening approach. Interestingly, when comparing the phenotypes (nuclear area and mitotic index) across the different processes we found that they affected the phenotypes differently (Supplemental Figure 2B-D), which confirmed the previous observation that the measurement of different phenotypes was required to be able to assay different cell cycle processes.

The genome-wide screen identified many components with phenotypes similar to those of known cell cycle regulators (Figure 2A-E). We attempted to use genetic interaction analysis to elucidate their functional relationship with the known cell cycle machinery. To this end we selected genes from the genome-wide screen that were expressed and displayed mitotic index and nuclear area phenotypes, prioritizing genes that had not been linked to cell cycle regulation previously (Bettencourt-Dias *et al.*, 2004; Bjorklund *et al.*, 2006; Kondo and Perrimon, 2011). We also excluded genes that were not conserved in humans, as well as genes with strong viability defects (for details of candidate selection see Supplemental Methods). This left us with 275 potential novel modulators from the genome-wide screen to be subjected to genetic interaction analysis: 238 with mitotic index phenotypes, and 37 with nuclear area phenotype (Supplemental Table S4). In addition we included several controls: genes with known roles in cell cycle regulation that also scored in the genome-wide screen, such as

components of the anaphase-promoting complex/cyclosome (APC/C) and the COP9 signalosome (CSN) complex, as well as genes that had no or only mild effects on the phenotypes of interest in order to prevent biases during the analysis of genetic interactions. Together, the list of candidates covered a broad range of mitotic index and nuclear area phenotypes, representative of the range of effects observed in the genome-wide screen (Figure 2F).

Different phenotypes identify non-redundant genetic interactions

To test the set of candidates from the genome-wide screen for genetic interactions we systematically co-depleted them with 14 known cell-cycle regulators ('query' genes, Supplemental Table S5) in all pairwise 'candidate x query' combinations. To reduce the influence of potential off-target effects on the interaction analysis we used two sequence-independent RNAi reagents to target each candidate and each query gene, resulting in overall 20,216 co-RNAi experiments with four independent measurements per gene pair. This experimental setup has been shown previously to allow robust estimation of single and double-RNAi phenotypes (Horn *et al.*, 2011). Genetic interactions and their significance were measured independently for each phenotype as deviations from the multiplicative model, which describes the expected combinatorial effect as the product of the single knockdown effects, and were summarized in π -scores (Supplemental Table S6).

For cell count, mitotic index and nuclear area phenotypes we observed a total of 1,419 genetic interactions at an experiment-wide false-discovery rate (FDR) of 1%. The mitotic index yielded an approximately 10 and 3-fold higher rate of genetic interactions than cell count and nuclear area, respectively (Figure 3A), which might be due to the phenotypes of the candidates that were mostly mitotic index effects (Supplemental Table S4). We assessed the node degree distribution for each phenotype (Figure 3B-D). The majority of genes had only few interactions ('1-3') independent of the phenotype. The number of positive and negative interactions tended to be unbalanced, and the strongest differences were seen for the mitotic index phenotype. Here, many genes had a few positive interactions (see '1-3' in Figure 3C), and a few genes had many negative interactions (see '7-9' in Figure 3C). By comparing the genetic interactions between phenotypes we found that only 31 gene pairs interacted in all three phenotypes. In contrast, 1,183 gene pairs (83.4%) displayed interactions specific for a single phenotype (Figure 3E). While genetic interactions between some known cell-cycle regulators, such as the members of the CSN complex, were observed in all three phenotypes (Figure 3F), other regulators, including the APC/C subunits *cdc23*, *ida*, *Apc10* and *fzy*, showed genetic interactions for the mitotic index phenotype only (Figure 3G). This indicated that measuring different cell-cycle relevant phenotypes might be required to connect novel genes to known processes.

Phenotype-specific interaction networks functionally connect candidate genes

To systematically predict functional associations of candidate genes, we assessed the similarity of their genetic interaction profiles. This type of analysis has been previously shown to provide robust approximations of functional associations (Costanzo *et al.*, 2010; Fuxman Bass *et al.*, 2013). We first calculated the Pearson correlation coefficient (PCC) between the interaction profiles of all candidates for each phenotype. To correct for genes that shared a high PCC with many genes, we transformed the PCC data into the connection specificity index (CSI) (Figure 4A), which reduces potential non-specific

similarities between genes by ranking the similarities according to the connectivity of their interaction partners (Green *et al.*, 2011; Fuxman Bass *et al.*, 2013).

We assessed whether the CSI improved functional associations between candidate genes compared to their single knockdown phenotypes. As expected, using the mitotic index all APC/C components tested (*ida*, *cdc23*, and *fzy*) had a high mitotic-index based CSI with *Apc10* (Figure 4B). In contrast, components of the Augmin complex (*wac*, *dgt2*) and the DREAM complex (*mip120*, *mip130*) shared a lower CSI with *Apc10*, despite their similar single knockdown effect on mitotic index (Figure 4B). Several other genes, such as the known modulator of mitosis *pont* (*pontin*, member of the INO80/SWR1 chromatin remodeling complexes) (Ducat *et al.*, 2008), also had a high CSI with *Apc10* without increasing the mitotic index when depleted alone (Figure 4B), drawing a potential connection to the APC/C. We also compared the nuclear-area based CSI of the cytokinesis regulator *Rho1* to the single knockdown effects of all other genes. This highlighted many known cytokinesis factors (e.g. *tum*, *zip*, *Det*), but deprioritized others, likely functionally independent genes that also showed an increased nuclear area, such as *tsr* (*twinstar*, *Drosophila* cofilin) a component required for mitotic telophase and cytokinesis (Gunsalus *et al.*, 1995) (Figure 4C). Together, this showed that the CSI could highlight genes with similar functions that could not be differentiated based on their single knockdown effects.

To identify association more systematically for each phenotype we placed all candidate genes in a force-directed network according to their functional similarity (CSI) (Figure 5A-B, S5A). The mitotic-index based network associated the APC/C with components facilitating mitotic spindle organization and regulation including dynein subunits (Arp87C) and the CCT chaperonin complex member Cct5 (Figure 5A). These close associations with the APC/C were not seen for the other phenotypes (Figure 5B, S5A-B). In the proximity of APC/C we observed additional interesting connections. We already highlighted the high CSI of the INO80/SWR1 complex member *pont* (*pontin*) with *Apc10*. We found more members of different chromatin remodeling complexes in the proximity of the APC/C, including *dom* (domino) and *Yeti* (both members of SWR1), *Nurf-38* (member of NURF complex), as well as *fs(1)h* (female sterile homeotic, a BET family protein). Further, several genes involved in regulation of transcription such as *pnt* (*pointed*, ETS transcription factor) and *l(2)NC136* (*Not3*, member of CCR4-NOT deadenylation complex) were connected to the APC/C. Together, this suggested a specific role for regulation of chromatin and transcription during mitosis (Morrison and Shen, 2009; Tanenbaum *et al.*, 2015). Other processes/complexes in the proximity of the APC/C included the DREAM complex (*mip120*, *mip130*), which has been previously shown to regulate mitotic events (Beall *et al.*, 2004; Georlette *et al.*, 2007), and the regulators of nuclear import *Nup107*, *Nup160* and *Kap-alpha3*. The latter finding suggested a role for nuclear pore complex components during mitosis that has been described before (Loiodice *et al.*, 2004). Other sub-networks highlighted known cell-cycle regulatory complexes, such as the CSN, but also processes that are less well understood in the context of the cell cycle, such as vesicle trafficking.

The mitotic-index based network failed to identify known functional associations between cytokinesis regulators (Figure 5A, S5C). In contrast, the nuclear-area based network connected *Rho1* with other components of cytokinesis (*tum*, *ial*, *Det*, *lin19*, and *zip*) (Figure 5B). Interestingly, several

regulators of vesicle trafficking and exocytosis were found in sub-networks connected to cytokinesis, suggesting a potential role of exocytosis during cytokinesis that has been previously described (Skop *et al.*, 2001). Although vesicle components grouped in the mitotic-index based network as well (e.g. *Arf72A*, *CG11753*, *Syx1A*), they were not connected directly to any of the other known processes, which highlights the information gain from generating phenotype-specific networks. Despite the conservation of some sub-networks across all three phenotypes, such as the CSN, or the APC/C, the connections between the processes and to uncharacterized genes were phenotype-specific. With mitotic-index based and nuclear-area based networks being stronger indicators of cell-cycle specific processes (Figure 5B-C) this provided us with testable hypothesis for potentially novel regulators of the cell cycle.

Golgi-resident and mRNA processing factors modulate mitotic progression

To assess the validity of our network-based prediction of gene functions we tested the role of two genes in cell-cycle relevant assays. The mitotic-index based network connected the APC/C and other regulators of mitosis to chromatin remodeling complexes and transcriptional regulators. We followed up on one of the genes in proximity to the APC/C, *l(2)NC136*, which is a member of the conserved deadenylation complex CCR4-NOT. Its human ortholog, *CNOT3*, has been shown to regulate mitotic progression by destabilizing the mRNA of the spindle assembly checkpoint (SAC) component *MAD1* (Takahashi *et al.*, 2012). To confirm the predicted role for *l(2)NC136* we knocked down the gene in *Drosophila* S2 cells with dsRNAs for four days and triggered a G₂/M checkpoint arrest by doxorubicin or etoposide treatment for 6 hours to allow cells with intact mitotic progression machinery to exit M-phase (Figure 5C). Cells depleted of *l(2)NC136* displayed a ~4-fold higher frequency of pH3-positive nuclei in both treatments compared to a control knockdown, indicating a delay in mitotic exit. To validate the conserved function of *l(2)NC136* in human cells we knocked down its ortholog, *CNOT3*, in HeLa cells using siRNAs, and assessed the cycle after release from a nocodazole-induced prometaphase arrest. Similarly to *Drosophila* cells, HeLa cells displayed a significant mitotic delay (assessed by quantifying G₂/M-phase contents; $p < 0.019$, paired Student's t-test) after knockdown of *CNOT3* (Figure 5D and S5D) compared to a control siRNA. These results confirmed a role of *l(2)NC136* during mitotic exit as was suggested by the network-based predictions.

Another process highlighted in both the mitotic-index based and nuclear-area based networks was vesicular trafficking. Several components of this network have been shown with cell-cycle specific functions previously. For example, *syntaxin1A* (*syx1A*), which encodes for a t-SNARE, was shown to be required for mitotic telophase (Somma *et al.*, 2002). *Gmap* and *Arf72A* are crucial for Golgi inheritance during cell division (Rios *et al.*, 2004; Eisman *et al.*, 2006). These genes formed a subgroup in the mitotic-index based network also containing the largely uncharacterized gene *CG11753* (Figure 5B). Its human ortholog, *SYS1*, has been shown with a function during golgi-targeted vesicular transport (Behnia *et al.*, 2004; Setty *et al.*, 2004). In agreement with its predicted role, depletion of both *CG11753* in *Drosophila* S2 cells or *SYS1* in HeLa cells delayed mitotic progression (Figure 5C-D).

The mitosis phenotypes seen for *l(2)NC136/CNOT3* and *CG11753/SYS1* in independent assays in *Drosophila* and human cells showed that hypothesis generated from mitotic-index or nuclear-area based interaction networks could be validated. Future studies could address more detailed how

regulation of transcription and vesicular traffic connect to cell cycle/mitosis. Further, additional sub-networks could be subjected to similar follow-up analysis to understand their role during the cell cycle.

Concluding remarks

This study demonstrates how unbiased, genome-wide screening followed by genetic interaction analysis can fine-tune predictions of gene function and guide follow-up experimentation by providing more specific and testable hypotheses. Importantly, predictions of gene functions from interactions based on phenotypes relevant to the biology examined, such as mitotic index and nuclear area to assay cell cycle, were superior to predictions of gene functions from viability/cell-count based interactions. Genetic interaction networks based on relevant phenotypes reconstructed known functional relations during mitotic progression and cytokinesis and suggested potentially novel regulators. We validated novel roles for a mRNA processing component and a Golgi-vesicular transport protein during mitotic exit.

With automated imaging being a versatile tool to simultaneously record multiple quantitative phenotypes (Perlman *et al.*, 2005; Fuchs *et al.*, 2010; Fischer *et al.*, 2015) this approach could be expanded to other biological processes by assaying relevant markers. Established reporter-based readouts to monitor the activity of signaling pathways could also be used to perform genetic interaction analysis, and differential networks could be build from experiments using different ways to activate or suppress the pathway.

DATA ACCESS

Supplemental Tables S1-S7, Figures S1-S5, and Supplemental Material and Methods are available from the journal website and comprise all interaction (π -) scores and p-values.

METHODS

Drosophila tissue culture

We cultured Schneider S2 cells adjusted to serum-free growth medium (D.Mel-2; Invitrogen) in Express Five SFM (Invitrogen) supplemented with 20 mM GlutaMAX (Invitrogen) and 1% penicillin-streptomycin (Invitrogen).

RNAi library

We used a genome-wide RNAi library targeting ~98% of all coding genes in the *Drosophila* genome designed against FlyBase annotations for the *D. melanogaster* BDGP genome releases 4 and 5 using the NEXT-RNAi software (Horn *et al.*, 2010). In addition, the library covered 1,254 strongly expressed regions from the Heidelberg predictions (HDC) of *Drosophila* genes not covered by FlyBase (Hild *et al.*, 2003). Primer and dsRNA sequence information, target mappings as well as the analysis of specificity and additional features of the dsRNA designs are available through GenomeRNAi (www.genomernai.org) (Schmidt *et al.*, 2013). For screening, the library was aliquoted in 384-well plates (black/clear, BD Falcon) with an average of 250ng dsRNA per well in 5ul water.

Genome-wide RNAi screening

In each biological replicate, we seeded 6,500 cells in 40 μ l culture medium with 0.2 μ l of 0.4 mg ml⁻¹ DDAB per well (in black/clear 384-well plates, BD Falcon) and incubated the plates for 5 days at 25 °C before fixation, staining and imaging of cells.

Cell staining and imaging

Cell stainings were done using a Beckman Biomek FX robot with 384-well tip head. First, of the 40 μ l assay volume 15ul were removed and cells were fixed/permeabilized for 60min at room temperature by addition of 40 μ l of a 6% PFA (SIGMA), 0.3% TX-100 (AppliChem) solution in PBS (SIGMA). Cells were washed by removing 40 μ l supernatant and addition of 50 μ l PBS. Next, 50 μ l of the supernatant were removed and 10 μ l of a monoclonal Phospho-Histone H3 antibody (conjugated to Alexa Fluor 647, Cell Signaling, #3458) diluted 1:750 in 4% BSA (GERBU), 0.1% TX-100 (in PBS) were added and incubated overnight at 8°C (protected from light). The next day 10 μ l supernatant were removed and DNA was stained by addition of 40 μ l Hoechst 33342 (Invitrogen) diluted 1:2000 in PBS and incubation for 30min at room temperature. Finally, cells were washed once by removing 40 μ l supernatant and adding 50 μ l PBS and washed another two times by removing 50 μ l supernatant and adding 50 μ l PBS. Plates were sealed with aluminum sealing tape (Corning) and imaged directly or stored at 8°C until imaging. Fluorescence images were acquired on an IN Cell Analyzer 2000 (GE Healthcare) using a 4x Objective, which enables capturing the entire well in one image. One image was acquired for each of the two channels (Hoechst and phospho-Histone H3 antibody).

Image analysis

Image analysis and feature extraction from the 4x images (16bit, 2048x2048 pixels) was performed using the R/Bioconductor package EBImage (Pau *et al.*, 2010). The nuclei were segmented and identified separately for the Hoechst and phospho-H3 channels. Adaptive thresholding (width of moving window 4 pixels) was used to separate nuclei areas from the image background. Nuclei were identified by local maximum search on the fluorescence images. The nuclei areas were extended from the local maxima by a propagation algorithm (Jones *et al.*, 2005). Nearest neighbor search was used to match phospho-H3 objects to nuclei in the Hoechst channel (only mitotic nuclei were visible in the phospho-H3 channel). Matches were accepted if the distance between the centers of the objects in both channels was smaller than 5 pixels. 84 quantitative features were extracted, out of which we focused on three: nuclei count (a correlate of cell count), mitotic index (the ratio of nuclei in the phospho-H3 channel and the Hoechst channel), and nuclear area.

Computational analysis of the genome-wide RNAi screen

Raw data of each feature was first log₂-transformed. To account for row and/or column effects, a local polynomial regression (loess) on the spatial coordinates was fit to each plate and subtracted. Loess-normalized values were further adjusted for the plate variance, generating z-scores. Replicates were summarized for each feature by taking the median. We focused on three of the features: the number of

cells per well, the mitotic index and the average nuclear area. Overall, a non-linear trend between cell count and the other two phenotypes (nuclear area, mitotic index) was observed. We calculated a model (using loess regression) to adjust for cell count effect on these phenotypes and computed z-scores from the residuals (Supplemental Table S1). The heatmap of z-scores in Figure 2A was generated using hierarchical clustering based on Euclidean distances.

Combinatorial RNAi

For the double-RNAi screen, we used a candidate-sensitizer design. 125 ng (2.5 μ l) of each candidate dsRNAs were pipetted into a 384-well clear-bottom microscopy plate (BD Falcon) as described above. Then, 125 ng (2.5 μ l) of one of the sensitizer dsRNAs were added using a NanoDrop II dispenser (Innovadyne), creating \sim 21,000 combinations (28 sensitizer dsRNAs versus 750 candidate dsRNAs). Each pairwise combination of genes was assayed through four pairs of independent dsRNA designs: denote by A and A' \square the two independent designs targeting one gene and by B and B' \square the two independent dsRNA reagents targeting the other, then each biological replicate of the experiment contained the candidate-sensitizer combinations A-B, A-B', A'-B, A'-B'. In each well, 6,500 cells were seeded in 30 μ l culture medium with 0.15 μ l of 0.4 mg ml⁻¹ DDAB per well and incubated for 5 d at 25°C before fixation, staining and imaging of cells (using the methods described for the genome-wide screen).

Mathematical modeling of synthetic genetic interactions

As described previously (Axelsson *et al.*, 2011; Horn *et al.*, 2011) we used a multiplicative model as the reference model (null model), which assumes that the double RNAi phenotypic effect of non-interacting genes is equal to the product of the single RNAi phenotypic effects. The single RNAi phenotypic effects (main effects) for the 14 ‘query’ genes were estimated by taking the median effect over all candidate genes (per phenotype). To prevent biases for the main-effect estimates of candidate genes their main effects were estimated using measurements after the gene was co-depleted with control dsRNAs (targeting non-expressed Firefly luciferase). Pair-wise interaction scores were then computed as the log-ratio of the measured phenotype and the predicted phenotype (from the reference model), which is the product of the two single knock down effects. The significance of an interaction was assessed by calculating the deviation from zero from four interaction scores per gene pair (four independent co-RNAi experiments per gene pair). To this end a moderated t-test (R/Bioconductor package limma) was used, which first estimates the standard errors (SEM) by fitting a linear model through the four values, followed by empirical Bayes smoothing of the SEM (Smyth, 2004). P-values were adjusted for multiple testing by the method of Benjamini-Hochberg controlling the false discovery rate (FDR) (Benjamini and Hochberg, 1995).

Calculation of the connection specificity index on the similarity between genetic interaction profiles

The connectivity specificity index (CSI) is based on a correlation matrix. For each pair of target genes the Pearson correlation coefficient (PCC) of the two genetic interaction profiles along all query genes

was computed. The CSI of a gene pair A-B was then defined as the fraction of genes connected to A and B that have a PCC smaller than the PCC of A and B. A constant of 0.01 was applied in the CSI definition of (Green *et al.*, 2011).

Induction of G₂/M checkpoint arrest in *Drosophila* S2 cells

To test the mitotic arrest after RNAi against genes selected from the primary screen, we triggered G₂/M checkpoint arrest in *Drosophila* S2 cells 96 h past dsRNA transfection using 4 μ M doxorubicin or 20 μ M etoposide. After 6 h, cells were fixed and stained for their DNA content (Hoechst 33342) and for pH3, and their mitotic index phenotype was determined (for details see Supplemental Methods).

FACS-based analysis of mitotic exit in human HeLa cells

Human HeLa cells were transfected with siRNA pools targeting the gene of interest and cultured for 3d under standard conditions. A prometaphase arrest was induced applying 40 ng/ml nocodazole for 18 h under standard conditions, and cells were released from this arrest and fixed at different time points up to 8 h post release. After propidium iodide staining, cell cycle profiles were determined using FACS analysis, counting 10,000 events per sample (for details see Supplemental Methods).

AUTHOR CONTRIBUTIONS

MBi, TH, TS, WH and MB designed the experiments. MBi, TH and TS performed the experiments. MBi, TH and BF performed the analysis. MBi, TH, BF, TS, WH and MB wrote the manuscript. All authors have read and approved the manuscript for publication.

ACKNOWLEDGEMENT

We thank the members of the Boutros and Huber labs for helpful discussions and Y. Kimata for comments on the manuscript. T.S. was supported by a CellNetworks postdoctoral fellowship, T.H. by a fellowship from the Studienstiftung. M.Bi. is supported by a Ph.D. fellowship from the Helmholtz International Graduate School for Cancer Research. Research in the laboratory of M.B. is supported by grants from the European Research Council (ERC) and the Helmholtz Society. W.H. and B.F. acknowledge funding from the European Commission NoE Systems Microscopy.

REFERENCES

Axelsson, E., Sandmann, T., Horn, T., Boutros, M., Huber, W., and Fischer, B. (2011). Extracting quantitative genetic interaction phenotypes from matrix combinatorial RNAi. *BMC Bioinformatics* 12, 342.

Bakal, C., Linding, R., Llense, F., Heffern, E., Martin-Blanco, E., Pawson, T., and Perrimon, N. (2008). Phosphorylation networks regulating JNK activity in diverse genetic backgrounds. *Science* 322, 453-456.

Beall, E.L., Bell, M., Georlette, D., and Botchan, M.R. (2004). Dm-myb mutant lethality in *Drosophila* is dependent upon mip130: positive and negative regulation of DNA replication. *Genes Dev* 18, 1667-1680.

Behnia, R., Panic, B., Whyte, J.R., and Munro, S. (2004). Targeting of the Arf-like GTPase Arl3p to the Golgi requires N-terminal acetylation and the membrane protein Sys1p. *Nat Cell Biol* 6, 405-413.

Benjamini, Y., and Hochberg, Y. (1995). Controlling the False Discovery Rate: A Practical and Powerful Approach to Multiple Testing. *J R Stat Soc Series B Stat Methodol* 57, 289-300.

Bettencourt-Dias, M., Giet, R., Sinka, R., Mazumdar, A., Lock, W.G., Balloux, F., Zafiropoulos, P.J., Yamaguchi, S., Winter, S., Carthew, R.W., Cooper, M., Jones, D., Frenz, L., and Glover, D.M. (2004). Genome-wide survey of protein kinases required for cell cycle progression. *Nature* *432*, 980-987.

Bjorklund, M., Taipale, M., Varjosalo, M., Saharinen, J., Lahdenpera, J., and Taipale, J. (2006). Identification of pathways regulating cell size and cell-cycle progression by RNAi. *Nature* *439*, 1009-1013.

Boutros, M., and Ahringer, J. (2008). The art and design of genetic screens: RNA interference. *Nat Rev Genet* *9*, 554-566.

Boutros, M., Kiger, A.A., Armknecht, S., Kerr, K., Hild, M., Koch, B., Haas, S.A., Paro, R., and Perrimon, N. (2004). Genome-wide RNAi analysis of growth and viability in Drosophila cells. *Science* *303*, 832-835.

Carmena, M., Wheelock, M., Funabiki, H., and Earnshaw, W.C. (2012). The chromosomal passenger complex (CPC): from easy rider to the godfather of mitosis. *Nat Rev Mol Cell Biol* *13*, 789-803.

Carpenter, A.E., and Sabatini, D.M. (2004). Systematic genome-wide screens of gene function. *Nat Rev Genet* *5*, 11-22.

Chew, S.K., Rad, R., Futreal, P.A., Bradley, A., and Liu, P. (2011). Genetic screens using the piggyBac transposon. *Methods* *53*, 366-371.

Collins, S.R., Miller, K.M., Maas, N.L., Roguev, A., Fillingham, J., Chu, C.S., Schuldiner, M., Gebbia, M., Recht, J., Shales, M., Ding, H., Xu, H., Han, J., Ingvarsottir, K., Cheng, B., Andrews, B., Boone, C., Berger, S.L., Hieter, P., Zhang, Z., Brown, G.W., Ingles, C.J., Emili, A., Allis, C.D., Toczyski, D.P., Weissman, J.S., Greenblatt, J.F., and Krogan, N.J. (2007). Functional dissection of protein complexes involved in yeast chromosome biology using a genetic interaction map. *Nature* *446*, 806-810.

Costanzo, M., Baryshnikova, A., Bellay, J., Kim, Y., Spear, E.D., Sevier, C.S., Ding, H., Koh, J.L., Toufighi, K., Mostafavi, S., Prinz, J., St Onge, R.P., VanderSluis, B., Makhnevych, T., Vizeacoumar, F.J., Alizadeh, S., Bahr, S., Brost, R.L., Chen, Y., Cokol, M., Deshpande, R., Li, Z., Lin, Z.Y., Liang, W., Marback, M., Paw, J., San Luis, B.J., Shuteriqi, E., Tong, A.H., van Dyk, N., Wallace, I.M., Whitney, J.A., Weirauch, M.T., Zhong, G., Zhu, H., Houry, W.A., Brudno, M., Ragibizadeh, S., Papp, B., Pal, C., Roth, F.P., Giaever, G., Nislow, C., Troyanskaya, O.G., Bussey, H., Bader, G.D., Gingras, A.C., Morris, Q.D., Kim, P.M., Kaiser, C.A., Myers, C.L., Andrews, B.J., and Boone, C. (2010). The genetic landscape of a cell. *Science* *327*, 425-431.

DasGupta, R., Kaykas, A., Moon, R.T., and Perrimon, N. (2005). Functional genomic analysis of the Wnt-wingless signaling pathway. *Science* *308*, 826-833.

Dixon, S.J., Fedyshyn, Y., Koh, J.L., Prasad, T.S., Chahwan, C., Chua, G., Toufighi, K., Baryshnikova, A., Hayles, J., Hoe, K.L., Kim, D.U., Park, H.O., Myers, C.L., Pandey, A., Durocher, D., Andrews, B.J., and Boone, C. (2008). Significant conservation of synthetic lethal genetic interaction networks between distantly related eukaryotes. *Proc Natl Acad Sci U S A* *105*, 16653-16658.

Dominski, Z., Yang, X.C., Purdy, M., Wagner, E.J., and Marzluff, W.F. (2005). A CPSF-73 homologue is required for cell cycle progression but not cell growth and interacts with a protein having features of CPSF-100. *Mol Cell Biol* *25*, 1489-1500.

Doronkin, S., Djagaeva, I., and Beckendorf, S.K. (2003). The COP9 signalosome promotes degradation of Cyclin E during early Drosophila oogenesis. *Dev Cell* *4*, 699-710.

Ducat, D., Kawaguchi, S., Liu, H., Yates, J.R., 3rd, and Zheng, Y. (2008). Regulation of microtubule assembly and organization in mitosis by the AAA+ ATPase Pontin. *Mol Biol Cell* *19*, 3097-3110.

Echard, A., Hickson, G.R., Foley, E., and O'Farrell, P.H. (2004). Terminal cytokinesis events uncovered after an RNAi screen. *Curr Biol* *14*, 1685-1693.

Eisman, R.C., Stewart, N., Miller, D., and Kaufman, T.C. (2006). centrosomin's beautiful sister (cbs) encodes a GRIP-domain protein that marks Golgi inheritance and functions in the centrosome cycle in Drosophila. *J Cell Sci* *119*, 3399-3412.

Fischer, B., Sandmann, T., Horn, T., Billmann, M., Chaudhary, V., Huber, W., and Boutros, M. (2015). A map of directional genetic interactions in a metazoan cell. *Elife* *4*.

Fuchs, F., Pau, G., Kranz, D., Sklyar, O., Budjan, C., Steinbrink, S., Horn, T., Pedal, A., Huber, W., and Boutros, M. (2010). Clustering phenotype populations by genome-wide RNAi and multiparametric imaging. *Mol Syst Biol* *6*, 370.

Fuxman Bass, J.I., Diallo, A., Nelson, J., Soto, J.M., Myers, C.L., and Walhout, A.J. (2013). Using networks to measure similarity between genes: association index selection. *Nat Methods* *10*, 1169-1176.

Georlette, D., Ahn, S., MacAlpine, D.M., Cheung, E., Lewis, P.W., Beall, E.L., Bell, S.P., Speed, T., Manak, J.R., and Botchan, M.R. (2007). Genomic profiling and expression studies reveal both positive

and negative activities for the Drosophila Myb MuvB/dREAM complex in proliferating cells. *Genes Dev* 21, 2880-2896.

Goshima, G., and Kimura, A. (2010). New look inside the spindle: microtubule-dependent microtubule generation within the spindle. *Curr Opin Cell Biol* 22, 44-49.

Green, R.A., Kao, H.L., Audhya, A., Arur, S., Mayers, J.R., Fridolfsson, H.N., Schulman, M., Schloissnig, S., Niessen, S., Laband, K., Wang, S., Starr, D.A., Hyman, A.A., Schedl, T., Desai, A., Piano, F., Gunsalus, K.C., and Oegema, K. (2011). A high-resolution *C. elegans* essential gene network based on phenotypic profiling of a complex tissue. *Cell* 145, 470-482.

Gunsalus, K.C., Bonaccorsi, S., Williams, E., Verni, F., Gatti, M., and Goldberg, M.L. (1995). Mutations in *twinstar*, a Drosophila gene encoding a cofilin/ADF homologue, result in defects in centrosome migration and cytokinesis. *J Cell Biol* 131, 1243-1259.

Hild, M., Beckmann, B., Haas, S.A., Koch, B., Solovyev, V., Busold, C., Fellenberg, K., Boutros, M., Vingron, M., Sauer, F., Hoheisel, J.D., and Paro, R. (2003). An integrated gene annotation and transcriptional profiling approach towards the full gene content of the Drosophila genome. *Genome Biol* 5, R3.

Horn, T., and Boutros, M. (2013). Design of RNAi reagents for invertebrate model organisms and human disease vectors. *Methods Mol Biol* 942, 315-346.

Horn, T., Sandmann, T., and Boutros, M. (2010). Design and evaluation of genome-wide libraries for RNA interference screens. *Genome Biol* 11, R61.

Horn, T., Sandmann, T., Fischer, B., Axelsson, E., Huber, W., and Boutros, M. (2011). Mapping of signaling networks through synthetic genetic interaction analysis by RNAi. *Nat Methods* 8, 341-346.

Jones, T., Carpenter, A., and Golland, P. (2005). Voronoi-based segmentation of cells on image manifolds. *Computer Vision for Biomedical Image Applications*, 535-543.

Jonikas, M.C., Collins, S.R., Denic, V., Oh, E., Quan, E.M., Schmid, V., Weibezahl, J., Schwappach, B., Walter, P., Weissman, J.S., and Schuldiner, M. (2009). Comprehensive characterization of genes required for protein folding in the endoplasmic reticulum. *Science* 323, 1693-1697.

Jorgensen, E.M., and Mango, S.E. (2002). The art and design of genetic screens: *caenorhabditis elegans*. *Nat Rev Genet* 3, 356-369.

Kiger, A.A., Baum, B., Jones, S., Jones, M.R., Coulson, A., Echeverri, C., and Perrimon, N. (2003). A functional genomic analysis of cell morphology using RNA interference. *J Biol* 2, 27.

Kittler, R., Putz, G., Pelletier, L., Poser, I., Heninger, A.K., Drechsel, D., Fischer, S., Konstantinova, I., Habermann, B., Grabner, H., Yaspo, M.L., Himmelbauer, H., Korn, B., Neugebauer, K., Pisabarro, M.T., and Buchholz, F. (2004). An endoribonuclease-prepared siRNA screen in human cells identifies genes essential for cell division. *Nature* 432, 1036-1040.

Kondo, S., and Perrimon, N. (2011). A genome-wide RNAi screen identifies core components of the G-M DNA damage checkpoint. *Sci Signal* 4, rs1.

Laufer, C., Fischer, B., Billmann, M., Huber, W., and Boutros, M. (2013). Mapping genetic interactions in human cancer cells with RNAi and multiparametric phenotyping. *Nat Methods* 10, 427-431.

Lehner, B., Crombie, C., Tischler, J., Fortunato, A., and Fraser, A.G. (2006). Systematic mapping of genetic interactions in *Caenorhabditis elegans* identifies common modifiers of diverse signaling pathways. *Nat Genet* 38, 896-903.

Loiodice, I., Alves, A., Rabut, G., Van Overbeek, M., Ellenberg, J., Sibarita, J.B., and Doye, V. (2004). The entire Nup107-160 complex, including three new members, is targeted as one entity to kinetochores in mitosis. *Mol Biol Cell* 15, 3333-3344.

Manley, J.L. (1995). A complex protein assembly catalyzes polyadenylation of mRNA precursors. *Curr Opin Genet Dev* 5, 222-228.

Morrison, A.J., and Shen, X. (2009). Chromatin remodelling beyond transcription: the INO80 and SWR1 complexes. *Nat Rev Mol Cell Biol* 10, 373-384.

Musacchio, A., and Salmon, E.D. (2007). The spindle-assembly checkpoint in space and time. *Nature reviews Molecular cell biology* 8, 379-393.

Nurminsky, D.I., Nurminskaya, M.V., De Aguiar, D., and Hartl, D.L. (1998). Selective sweep of a newly evolved sperm-specific gene in Drosophila. *Nature* 396, 572-575.

Pan, X., Yuan, D.S., Xiang, D., Wang, X., Sookhai-Mahadeo, S., Bader, J.S., Hieter, P., Spencer, F., and Boeke, J.D. (2004). A robust toolkit for functional profiling of the yeast genome. *Mol Cell* 16, 487-496.

Patton, E.E., and Zon, L.I. (2001). The art and design of genetic screens: zebrafish. *Nat Rev Genet* 2, 956-966.

Pau, G., Fuchs, F., Sklyar, O., Boutros, M., and Huber, W. (2010). EBImage--an R package for image processing with applications to cellular phenotypes. *Bioinformatics* 26, 979-981.

Perlman, Z.E., Mitchison, T.J., and Mayer, T.U. (2005). High-content screening and profiling of drug activity in an automated centrosome-duplication assay. *ChemBioChem* 6, 145-151.

Rad, R., Rad, L., Wang, W., Cadinanos, J., Vassiliou, G., Rice, S., Campos, L.S., Yusa, K., Banerjee, R., Li, M.A., de la Rosa, J., Strong, A., Lu, D., Ellis, P., Conte, N., Yang, F.T., Liu, P., and Bradley, A. (2010). PiggyBac transposon mutagenesis: a tool for cancer gene discovery in mice. *Science* 330, 1104-1107.

Rios, R.M., Sanchis, A., Tassin, A.M., Fedriani, C., and Bornens, M. (2004). GMAP-210 recruits gamma-tubulin complexes to cis-Golgi membranes and is required for Golgi ribbon formation. *Cell* 118, 323-335.

Roguev, A., Bandyopadhyay, S., Zofall, M., Zhang, K., Fischer, T., Collins, S.R., Qu, H., Shales, M., Park, H.O., Hayles, J., Hoe, K.L., Kim, D.U., Ideker, T., Grewal, S.I., Weissman, J.S., and Krogan, N.J. (2008). Conservation and rewiring of functional modules revealed by an epistasis map in fission yeast. *Science* 322, 405-410.

Roguev, A., Talbot, D., Negri, G.L., Shales, M., Cagney, G., Bandyopadhyay, S., Panning, B., and Krogan, N.J. (2013). Quantitative genetic-interaction mapping in mammalian cells. *Nat Methods* 10, 432-437.

Schmidt, E.E., Pelz, O., Buhlmann, S., Kerr, G., Horn, T., and Boutros, M. (2013). GenomeRNAi: a database for cell-based and in vivo RNAi phenotypes, 2013 update. *Nucleic Acids Res* 41, D1021-1026.

Schuldiner, M., Collins, S.R., Thompson, N.J., Denic, V., Bhamidipati, A., Punna, T., Ihmels, J., Andrews, B., Boone, C., Greenblatt, J.F., Weissman, J.S., and Krogan, N.J. (2005). Exploration of the function and organization of the yeast early secretory pathway through an epistatic miniaarray profile. *Cell* 123, 507-519.

Setty, S.R., Strohlic, T.I., Tong, A.H., Boone, C., and Burd, C.G. (2004). Golgi targeting of ARF-like GTPase Arl3p requires its Nalpha-acetylation and the integral membrane protein Sys1p. *Nat Cell Biol* 6, 414-419.

Skop, A.R., Bergmann, D., Mohler, W.A., and White, J.G. (2001). Completion of cytokinesis in *C. elegans* requires a brefeldin A-sensitive membrane accumulation at the cleavage furrow apex. *Curr Biol* 11, 735-746.

Smyth, G.K. (2004). Linear models and empirical bayes methods for assessing differential expression in microarray experiments. *Stat Appl Genet Mol Biol* 3, Article3.

Somma, M.P., Fasulo, B., Cenci, G., Cundari, E., and Gatti, M. (2002). Molecular dissection of cytokinesis by RNA interference in *Drosophila* cultured cells. *Mol Biol Cell* 13, 2448-2460.

St Johnston, D. (2002). The art and design of genetic screens: *Drosophila melanogaster*. *Nat Rev Genet* 3, 176-188.

Takahashi, A., Kikuguchi, C., Morita, M., Shimodaira, T., Tokai-Nishizumi, N., Yokoyama, K., Ohsugi, M., Suzuki, T., and Yamamoto, T. (2012). Involvement of CNOT3 in mitotic progression through inhibition of MAD1 expression. *Biochem Biophys Res Commun* 419, 268-273.

Tanenbaum, M.E., Stern-Ginossar, N., Weissman, J.S., and Vale, R.D. (2015). Regulation of mRNA translation during mitosis. *Elife* 4.

Teixido-Travesa, N., Roig, J., and Luders, J. (2012). The where, when and how of microtubule nucleation - one ring to rule them all. *J Cell Sci* 125, 4445-4456.

Tischler, J., Lehner, B., and Fraser, A.G. (2008). Evolutionary plasticity of genetic interaction networks. *Nat Genet* 40, 390-391.

Tong, A.H., Lesage, G., Bader, G.D., Ding, H., Xu, H., Xin, X., Young, J., Berriz, G.F., Brost, R.L., Chang, M., Chen, Y., Cheng, X., Chua, G., Friesen, H., Goldberg, D.S., Haynes, J., Humphries, C., He, G., Hussein, S., Ke, L., Krogan, N., Li, Z., Levinson, J.N., Lu, H., Menard, P., Munyana, C., Parsons, A.B., Ryan, O., Tonikian, R., Roberts, T., Sdicu, A.M., Shapiro, J., Sheikh, B., Suter, B., Wong, S.L., Zhang, L.V., Zhu, H., Burd, C.G., Munro, S., Sander, C., Rine, J., Greenblatt, J., Peter, M., Bretscher, A., Bell, G., Roth, F.P., Brown, G.W., Andrews, B., Bussey, H., and Boone, C. (2004). Global mapping of the yeast genetic interaction network. *Science* 303, 808-813.

Wang, X., Fu, A.Q., McNerney, M.E., and White, K.P. (2014). Widespread genetic epistasis among cancer genes. *Nat Commun* 5, 4828.

Yeh, S.D., Do, T., Abbassi, M., and Ranz, J.M. (2012). Functional relevance of the newly evolved sperm dynein intermediate chain multigene family in *Drosophila melanogaster* males. *Commun Integr Biol* 5, 462-465.

Zavortink, M., Contreras, N., Addy, T., Bejsovec, A., and Saint, R. (2005). Tum/RacGAP50C provides a critical link between anaphase microtubules and the assembly of the contractile ring in *Drosophila melanogaster*. *J Cell Sci* 118, 5381-5392.

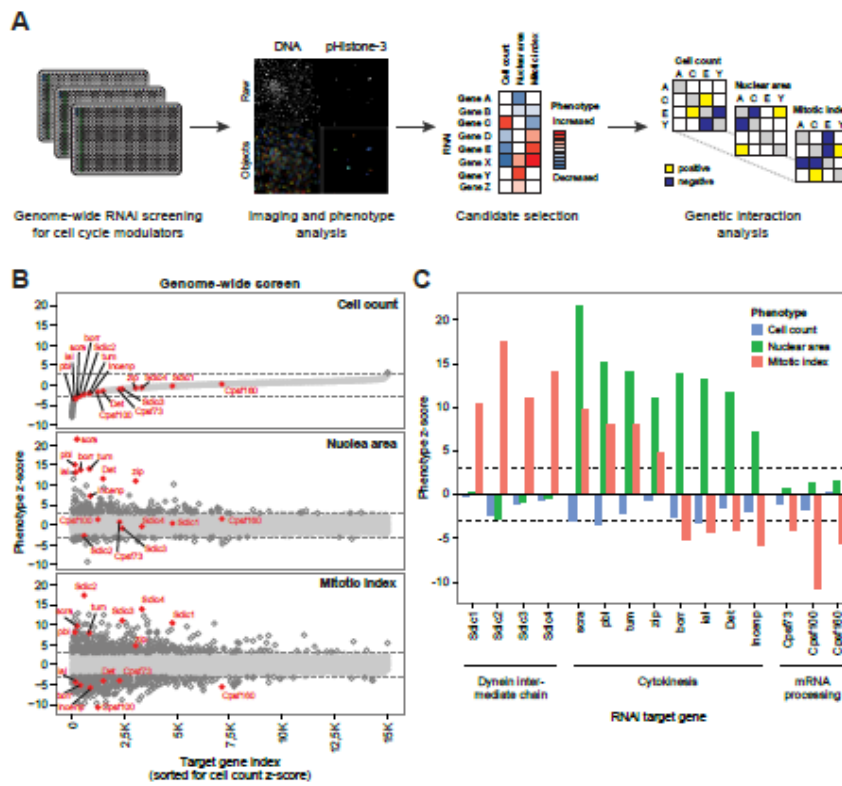


Figure 1

Figure 1: Combined genome-wide RNAi and synthetic genetic interaction analysis setup using multiple phenotypic readouts. (A) Genome-wide RNAi screening and high-throughput imaging to quantify the number of cells, nuclear area, and mitotic index are used to identify cell cycle regulators, which are further characterized by genetic interaction analysis. See text for details. (B) Comparison of the three phenotypes across the genome-wide dataset. The knockdown conditions (x-axis) are sorted according to their cell count phenotype (upper panel). Nuclear area (middle panel) and mitotic index (lower panel) phenotypes are shown in the same order. Highlighted in red are proteins that show differential effects across the phenotypes. Dashed lines indicate z-score cut-offs of 3 and -3 (points below the cut-offs are light grey, points above dark grey). (C) Barplots comparing the phenotypes (per functional group) for the knockdowns highlighted in B. Knockdowns of dynein intermediate chain proteins and mRNA processing factors show opposing effects on mitotic index, and have no effects on the other phenotypes. Knockdowns of proteins required for cytokinesis all increase the nuclear area, while they have opposing effects on mitotic index. Dashed lines indicate z-score cut-offs of 3 and -3.

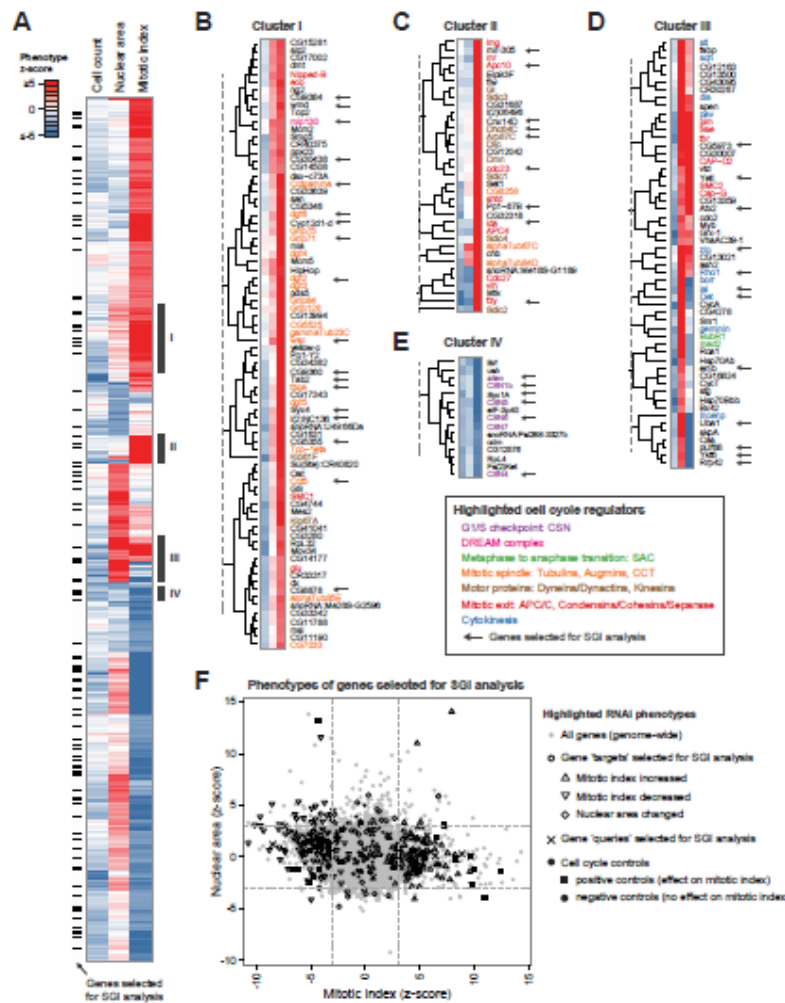


Figure 2

Figure 2: Genome-wide RNAi screening identifies known and potential novel regulators of cell cycle. (A) Heatmap of z-scores for 1,018 genes with an absolute z-score ≥ 3 in nuclear area and/or mitotic index after hierarchical clustering. Black bars to the left of the heatmap highlight genes that were selected for the synthetic genetic interaction (SGI) analysis. Bars on the right of the heatmap highlight clusters of genes that are enriched for factors with known roles in cell cycle and are shown in greater detail in panels B-E. (B-E) Detailed heatmaps of the clusters highlighted in A. Colors of gene names indicate their membership to certain groups of cell cycle regulators (see box). Arrows highlight genes that were selected for SGI analysis. See text for details. (F) Scatter plot of nuclear area and mitotic index phenotypes for genes selected for SGI analysis (black) on top of the genome-wide data (grey). The distribution of candidates and controls selected for the SGI analysis shows that it is representative of the effect range observed in the genome wide screen. Different types of candidates and controls are indicated by shape (see legend and Supplemental Tables S4-S5). CSN: COP9

signalosome, SAC: Spindle assembly checkpoint, CCT: cytosolic chaperonin containing t-complex, APC/C: anaphase-promoting complex/cyclosome.

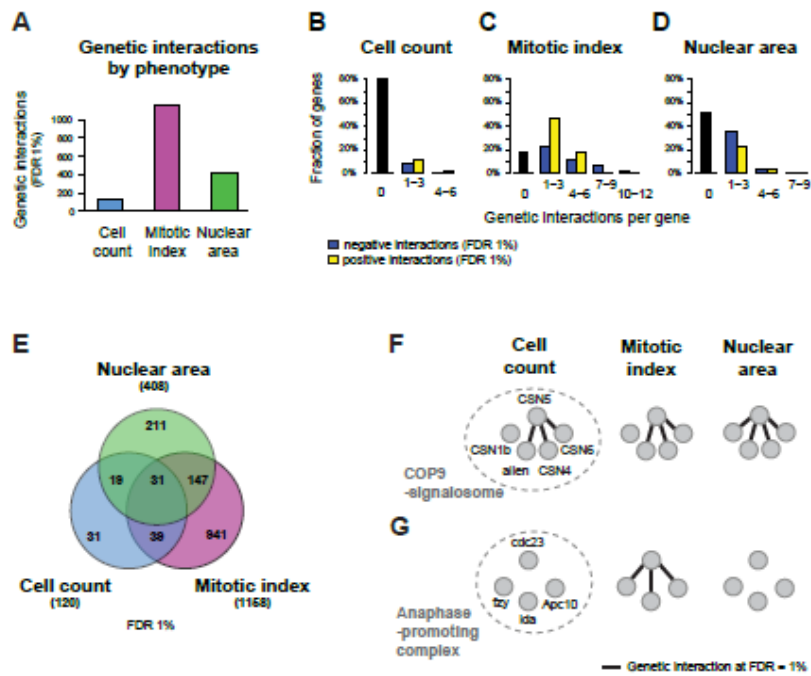


Figure 3

Figure 3: Genetic interactions across different phenotypes. (A) Comparing the number of genetic interactions affecting cell count, mitotic index or nuclear area shows that the majority of interactions are found for the mitotic index phenotype. Interactions were estimated from a set of 14 ‘query’ genes, and 350 ‘candidate’ genes/controls. (B-D) Node degree distributions showing number of positive (yellow bars) and negative (blue bars) genetic interactions per phenotype and on a per-gene basis. (E) A Venn diagram shows that there are overlapping, but also many exclusive genetic interactions between the phenotypes. (F, G) Genetic interactions within the COP9 signalosome (CSN) largely overlap between the phenotypes (F), while genetic interactions within the anaphase-promoting complex / cyclosome (APC/C) are exclusive to the mitotic index (G). In F and G all genetic interactions are alleviating, i.e. were less severe than expected according to the reference model. All genetic interactions were called at a false discovery rate (FDR) of 1%.

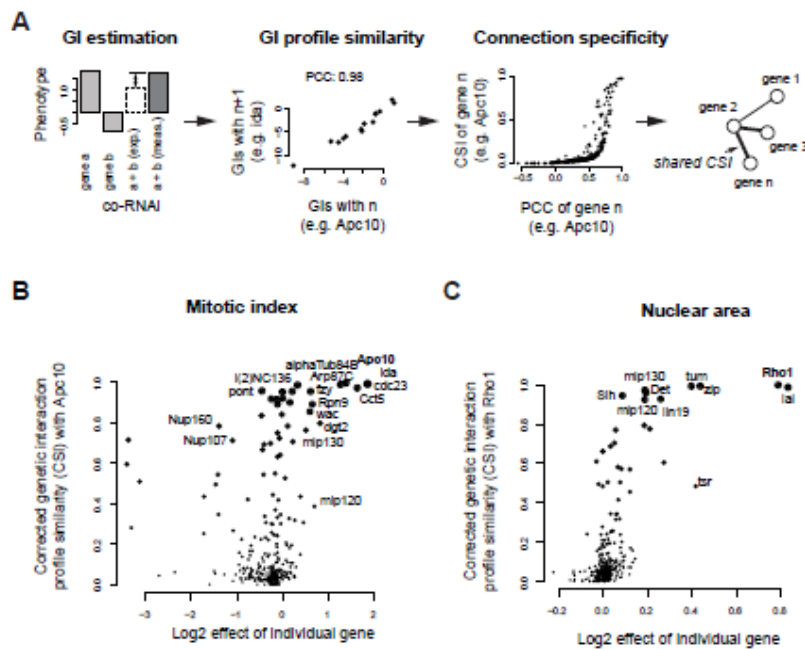


Figure 4

Figure 4: Genetic interaction profiles associate genes with similar functions. (A) Processing of genetic interaction profiles (GI) to predict functional similarity between genes. The profiles (14 π -scores) of each candidate gene pair were compared per phenotype by calculating the Pearson correlation coefficient (PCC). The example shows the PCC between the mitotic-index based profiles of the anaphase-promoting complex (APC/C) components *Apc10* and *ida*. The PCC was corrected by calculating the connection specificity index (CSI) with a correction factor / constant of 0.01. The example shows the relation between the PCC and CSI of *Apc10*. (B) A comparison of the mitotic-index based CSI connecting *Apc10* to all tested genes with the single knockdown effect of all genes shows additional APC/C components (and cell cycle regulators) in proximity to *Apc10*. (C) A comparison of the nuclear-area based CSI connecting *Rho1* to all tested genes with the single knockdown effect of all genes shows additional cytokinesis components (and cell cycle factors) in proximity to *Rho1*. See text for details. The point size is proportional to the CSI in B and C.

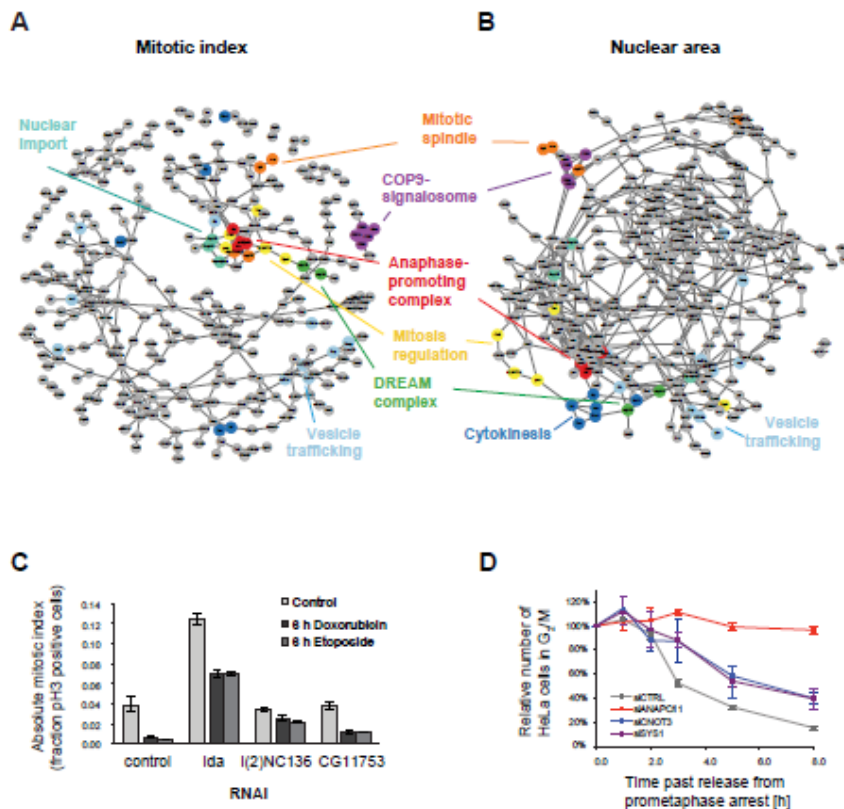


Figure 5

Figure 5: Networks based on cell-cycle relevant phenotypes. (A-B) Mitotic-index based (A) and nuclear-area based (B) functional associations of candidate genes show known cell cycle processes (different colors) linked to each other and to uncharacterized genes/processes. Genes were placed in a force-directed network based on the genetic interactions for each phenotype. Only gene pairs (connections) with connection specificity indices (CSI) > 0.95 are shown. (C) *I(2)NC136* and *CG11753* are required for mitotic progression in *Drosophila* cells. Each gene was knocked down by two independent dsRNA designs, *ida* was knocked down as positive control, and Firefly luciferase was used as negative control ('control'). 96 h past dsRNA transfection, the G2/M checkpoint was triggered by doxorubicin or etoposide, and cells were allowed to leave M-phase for 6h before assessing the mitotic index. The data shows the mean of 32 (control) or 4 (*ida*, *I(2)NC136*, *CG11753*) replicates, the error bars indicate s.e.m. (D) Functional depletion of the human orthologs of *I(2)NC136* and *CG11753* (*CNOT3* and *SYS1*, respectively) using siRNAs for 72h shows a delayed mitotic exit after release from prometaphase arrest in HeLa cells. Prometaphase arrest was induced by nocodazole treatment for 18h

and the fraction of G2/M cells was assessed at different time points after release by FACS analysis. The data shows the mean of 3 replicates, the error bars indicate s.e.m.